Purification of a single photon nonlinearity

H. Snijders,[1] J. A. Frey,[2] J. Norman,[3] M. P. Bakker,[1] A. Gossard,[3]
J. E. Bowers,[3] M. P. van Exter,[1] D. Bouwmeester,[1, 2] and W. Löffler[1]

[1]*Huygens–Kamerlingh Onnes Laboratory, Leiden University,*
P.O. Box 9504, 2300 RA Leiden, The Netherlands
[2]*Department of Physics, University of California, Santa Barbara, California 93106, USA*
[3]*Department of Electrical & Computer Engineering,*
University of California, Santa Barbara, California 93106, USA

We show that the lifetime-reduced fidelity of a semiconductor quantum dot–cavity single photon nonlinearity can be restored by polarization pre- and postselection. This is realized with a polarization degenerate microcavity in the weak coupling regime, where an output polarizer enables quantum interference of the two orthogonally polarized transmission amplitudes. This allows us to transform incident coherent light into a stream of strongly correlated photons with a second-order correlation function of $g^2(0) \gtrsim 40$, larger than previous experimental results even in the strong-coupling regime. This purification technique might also be useful to improve the fidelity of quantum dot based logic gates.

Single photon nonlinearities enabled by quantum two-level systems are essential for future quantum information technologies, as they are the building block of quantum photonics logic gates [1], deterministic entanglers of independent photons [2], and for coupling distant nodes to form a quantum network [3]. Near unity fidelity interaction of photons with a two level system such as an atom or quantum dot (QD) is enabled by embedding it into an optical cavity [4], where the electronic and photonic states become bound and form the dressed states [5] of cavity quantum electrodynamics (CQED). A hallmark of single photon nonlinearities is the modification of the photon statistics of a quasi-resonant weak coherent input beam [6]: First, the transmitted light photon statistics can become antibunched due to the photon blockade effect [1, 7, 8], which is enabled by the anharmonicity of the Jaynes-Cummings ladder [9–11]. Second, the system can be tuned to reach the regime of photon tunnelling [6, 12] where the single-photon component is reduced and photons are transmitted in $N > 1$ Fock states or "photon bundles" [13, 14].

In terms of the second-order photon correlation function $g^2(0)$, values up to ~ 2 [15–18] have been obtained experimentally with quantum dots, which hardly exceeds even the classical case of thermal light following Bose statistics of $g^2(0) = 2$. In atomic systems with much longer coherence times, values up to ~ 50 have been obtained [6], and it is known [19] that strict two-photon light sources exhibit diverging $g^2(0)$ if the two-photon flux is reduced. Most related quantum dot experiments to date have been operating in the strong-coupling regime of CQED, which is considered to be essential due to its photon-number dependent energy structure [6, 17, 18]. However, strong coupling requires a small optical mode volume, which in turn makes it extremely hard to achieve polarization degeneracy of the fundamental cavity mode. This is due to unavoidable deviations from the ideal shape and intrinsic birefringence [20, 21] on the GaAs platform, precluding implementation of de-
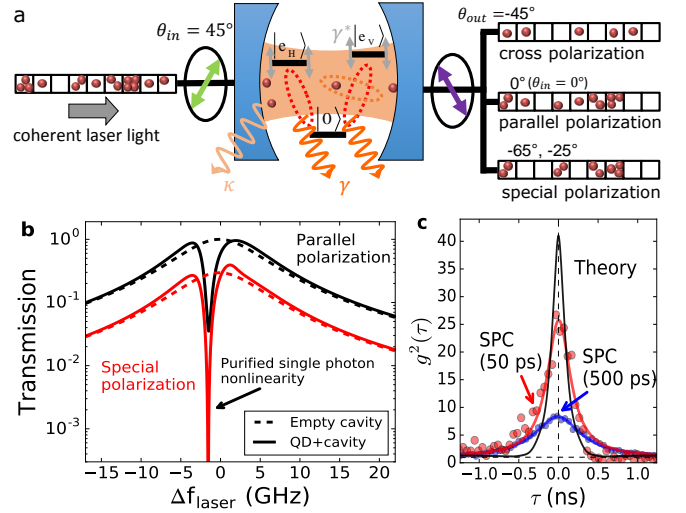

Figure 1. (a) Cartoon of the experiment: Polarization pre- and postselection in a resonant transmission CQED experiment enables tuning of the photon statistics from antibunched to bunched. (b) Theoretical resonant transmission spectra for coherent light with mean photon number $\ll 1$, with and without the quantum dot, comparing the conventional case (parallel polarizers) to the case of special polarization postselection along θ^*_{out}: close to one of the QD resonances, single-photon transmission is perfectly suppressed, despite the finite lifetime and cavity coupling of the QD transition. (c) Second-order correlation function (QD B) for the special polarization angle case, comparing theory and experiment using two different sets of single photon counters (SPCs) with different timing jitter, 50 ps and 500 ps.

terministic polarization-based quantum gates [2, 22, 23]. Here we show, using a polarization degenerate cavity in the weak coupling CQED regime, that we can transform incident coherent light into a stream of strongly correlated photons with $g^2(0) \gtrsim 25$, corresponding to $\gtrsim 40$ in the absence of detector jitter. The polarization degenerate cavity enables us to choose the incident polariza-

tion $\theta_{in} = 45°$ such that both fine-structure split quantum dot transitions along $\theta_{QD}^X = 90°$ and $\theta_{QD}^Y = 0°$ are excited, and we can use a postselection polarizer behind the cavity (θ_{out}) to induce quantum interference of the two transmitted orthogonal polarization components (Fig. 1a). This leads to the appearance of two special postselection polarizer angles $\theta_{out}^{*\pm}$ (depending on sample parameters), which can be used to restore perfect QD contrast (one of them is shown in Fig. 1b). This compensates fully for reduced QD-cavity coupling due to finite QD lifetime and QD-cavity coupling strength, leading to complete suppression of transmission of the single-photon component in the low excitation limit. The transmission of higher-photon number states remains largely intact, allowing us to observe in Fig. 1c the strongest photon correlations to date in a quantum dot system, even exceeding those of strongly coupled atomic systems [6]. In the following a detailed experimental and theoretical investigation of this effect, which can be seen as a purification of a single-photon nonlinearity, will be presented.

RESULTS

Device structure. Our device [24] consists of self-assembled InAs/GaAs quantum dots embedded in a micropillar Fabry-Perot cavity grown by molecular beam epitaxy [25]. The QD layer is embedded in a P-I-N junction, which enables tuning of the QD resonance frequency by the quantum confined Stark effect. For transverse mode confinement and to achieve polarization degenerate cavity modes, we first ion-etch micropillars of large diameter (35 μm) and slightly elliptical shape, then we use wet-chemical oxidation of an AlAs layer [26] to prepare an intra-cavity lens for transverse-mode confinement [27], avoiding loss by surface scattering at the side walls. Finally, we fine-tune the cavity modes by laser induced surface defects [28, 29] to obtain routinely a polarization mode splitting much less than 10% of the cavity linewidth. We show here data from two quantum dots, QD A and B, where QD A (B) is separated by a 20 nm (35 nm) tunnel barrier from the electron reservoir.

Device parameters and theoretical model. The system we study here is tuned to contain a single neutral QD within the cavity linewidth. The excitonic fine structure splitting leads to ≈ 2.5 GHz splitting between the orthogonally polarized QD transitions at $0°$ (ω_{QD}^Y) and $90°$ (ω_{QD}^X). To determine further system parameters, we model our QD-cavity system by a two-polarization Jaynes-Cummings (JC) Hamiltonian coupled to the incident coherent field, and take care of cavity and QD dissipation by the quantum master equation formalism [6, 30]. We compare experiment and theory for 6 different input-output polarizer settings to faithfully determine the model parameters [24]. For QD A we obtain

a cavity decay rate $\kappa = 69$ ns^{-1}, QD relaxation rate $\gamma_{||} = 3.5$ ns^{-1}, QD pure dephasing $\gamma^* = 6$ ns^{-1} , and QD-cavity coupling rate $g = 15$ ns^{-1}. These measurements were performed for an input power of 100 pW to avoid saturation effects. With this we can calculate the device cooperativity $C = \frac{g^2}{\kappa\gamma} = 0.4$ (with $\gamma = \frac{\gamma_{||}}{2} + \gamma^*$), which puts our system in the weak coupling regime. For QD B [Fig. 1 (c)] we obtain $\kappa = 105$ ns^{-1}, $g = 14$ ns^{-1}, $\gamma^{||} \approx 1.0$ $ns^{-1} \pm 0.3$ ns^{-1}, $\gamma^* \approx 0.7$ $ns^{-1} \pm 0.3$ ns^{-1}, leading to a enhanced cooperativity $C \approx 1.6 \pm 0.5$ ns^{-1}. Details are given in the supplemental information [24]. The cavity with QD B shows a residual polarization splitting of 4 GHz, which leads to less-perfect agreement of our theoretical model. Therefore we focus now on a different cavity with QD A having a lower maximal $g^2(0) \approx 3.7$ but with excellent agreement to theory.

Resonant photon correlation spectroscopy. We use a narrowband (100 kHz) laser to probe the system and study the transmitted light (Fig. 1a), as a function of incident polarization, frequency, and postselection polarizer angle behind the cavity. For each set of parameters, we measure the resonantly transmitted light intensity and its second-order photon correlation function $g^2(\tau)$ using a Hanbury Brown Twiss setup. The discrete nature of the QD levels leads to a strongly nonlinear response of the system depending on the incident photon number distribution; we operate at low intensities to avoid saturation effects. We show here only data for an incident polarization $\theta_{in} = 45°$, under which angle both QD transitions are equally excited, additional data is given in the supplemental information [24].

First, we compare experimental and theoretical resonant transmission measurements in Fig. 2, where the coherent-light transmittivity as a function of the laser detuning and orientation of the output polarizer angle θ_{out} is shown. For clarity, we have normalized the traces for each polarization setting. The horizontal red lines indicate the QD fine structure split transitions (ω_{QD}^X, ω_{QD}^Y), the black circles indicate regions of low transmission and the vertical dashed lines the special polarization angles $\theta_{out}^{*+} \approx -25°$, $\theta_{out}^{*-} \approx -65°$. From comparision of both panels in Fig. 2, we find excellent agreement between experiment and theory.

Now we perform photon correlation measurements; instead of tuning the laser, we now tune the QD. Because the cavity linewidth is large compared to the QD tuning range, a parameter space similar to that before is explored. Experimentally, using an external electric field to tune the QD via the quantum confined Stark effect is much more robust than laser frequency tuning. Fig. 3 shows the false-color map of $g^2(0)$ as function of output polarization θ_{out} and QD detuning. We see clearly that the enhanced bunching occurs under the special polarization condition in the low-transmittivity regions indicated in Fig. 2. This is expected as in weak coherent light beams, the P_1 single-photon component is dominating, and removal thereof should lead to enhanced bunching. The theoretical simulation (Fig. 3b) shows a maxi-
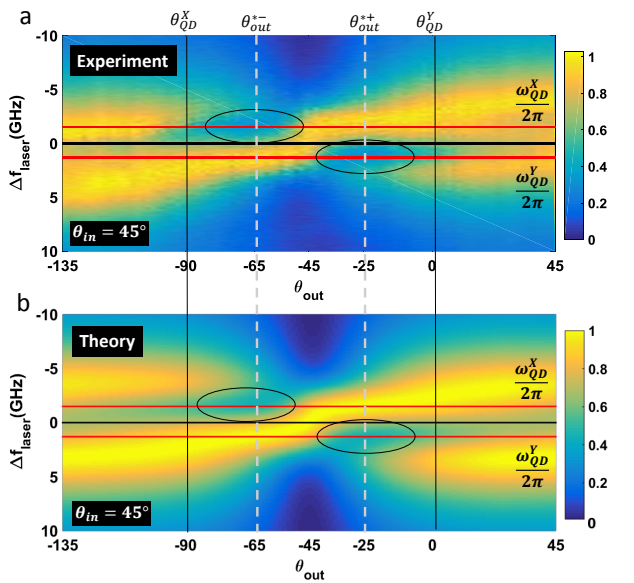
Figure 2. Experimental (a) and theoretical (b) false color plot of the columnwise normalized optical transmission as a function of the laser detuning Δf_{Laser} and the polarization θ_{out} ($\theta_{in} = 45°$). The fine-split QD transition frequencies are at $f_{QD}^X = -1.5$ GHz, $f_{QD}^Y = 1.3$ GHz. The black circles indicate the special polarization conditions with lowest transmission.
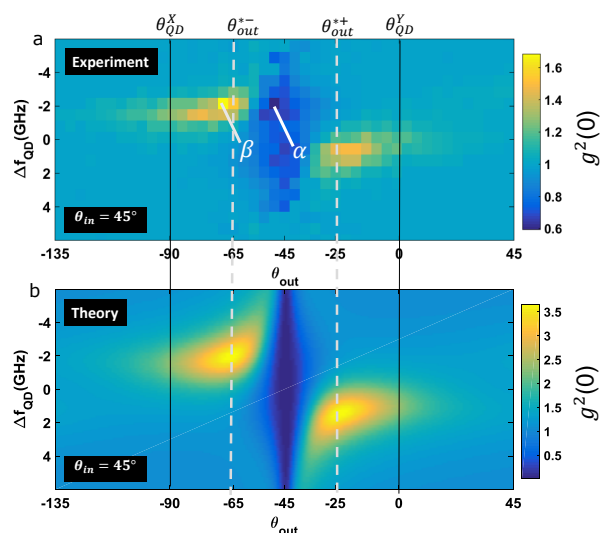

Figure 3. Experimental (a) and theoretical (b) data of the second-order correlation function as a function of the QD frequency and output polarization (θ_{out}). Green dashed lines indicate the special polarization angles, and α and β indicate the highest and lowest experimental $g^2(0)$ values, respectively.

mal photon bunching of $g^2(0) \approx 3.7$. Compared to this, the experimentally observed photon correlations are less (maximally $g^2(0) \approx 2.1$), but if we convolute the theoretical results with the detector response function, very good agreement is obtained (see supplemental information [24]). One also notices that the regions of high photon bunching exhibit hyperbolic shape, which is due to modification of the interference between the cavity and QD resonances while scanning the QD.

DISCUSSION

We have shown by experiment and theory that the reduced fidelity of a QD nonlinearity, caused by imperfect QD-cavity coupling, can be strongly enhanced by pre- and post-selection of specific polarization states. This enables transformation of a weak coherent input beam into highly bunched light with $g^2(0) \gtrsim 40$, a value that has not been reached before, not even in the strong coupling regime. To gain more insight, understanding in terms of the photon number distribution P_n is required, for which we use our theoretical model as direct experimental determination of P_n is strongly complicated by its sensitivity to loss. But also the simulation of narrowband photon number Fock input states is challenging in the quantum master model [32]. We continue here using coherent input light, and analyze the intra-cavity light in terms of its photon number distribution, however, taking full care of quantum interference at the postselection

polarizer. This polarizer leads to Hong-Ou-mandel type photon bunching similar to the case of a quantum beamsplitter, where the two polarization modes take over the role of the two input ports. We found that the photon statistics P_n can be calculated best by projection on the required Fock states using polarization-rotated Fock space ladder operators $b_{x/y}^\dagger = a_{x/y}^\dagger \cos\theta_{out} \mp a_{y/x}^\dagger \sin\theta_{out}$, and tracing out the undesired polarization component afterwards. For the numerically [6] calculated photonic density matrix operator ρ of our system, the photon number distribution after the polarizer becomes [33]:

$$P_n = \sum_{m=0}^{N} \frac{1}{n!\,m!} \langle 0_x 0_y | \left(b_x\right)^n \left(b_y\right)^m \rho \left(b_x^\dagger\right)^n \left(b_y^\dagger\right)^m |0_x 0_y\rangle$$

Fig. 4 shows the 4 lowest photon number probabilities as a function of the polarizer angle θ_{out}, for the case with and without quantum dot. In the bare cavity case we see, as expected, lowest transmission under the cross-polarization condition ($\theta_{out} = 45°$). For the case with the QD, we observe a photon-number dependent shift of the transmission dip. At the special polarization angle θ_{out}^*, we see that the one-photon component reaches a minimum while the higher-photon number states do not. Since $g^2(0) \propto 2P_2/P_1^2$ for $P_2 \ll P_1$ and $P_{n>2} \ll P_2$, the photon correlations diverge like $g^2(0) \propto 1/\alpha^2$ if the single-photon component is attenuated as $P_1 \to \alpha P_1$, explaining the enhanced photon bunching enabled by the purification technique.

It is important to note that also the two-photon transmission dip (P_2) is not exactly at cross-polarization, which suggests the following intuitive explanation: Ap-
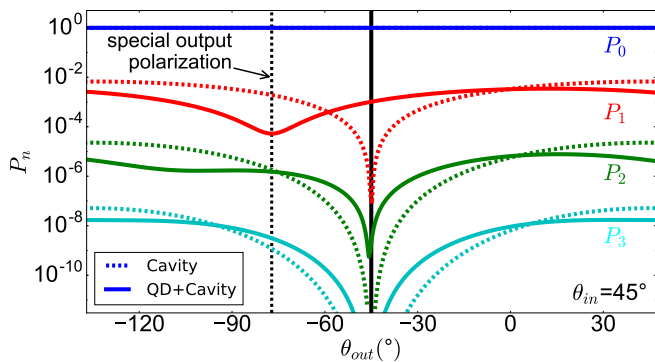
Figure 4. Calculated photon number distribution after the polarizer, with (through curves) and without (dashed curves) coupling to the quantum dot in the cavity, the laser frequency is set to one of the QD resonances. With QD, we clearly see the photon-number dependent shift of the transmission dip. Only the photon number distribution of the detected polarization component is shown, therefore the total number of photons in case with quantum dot can exceed the case without quantum dot due to polarization conversion by the dot. For clarity, pure dephasing has been neglected here, making the special polarization angle different from the previous simulations and experimental results.

parently, in the photon number basis, the different Fock states pick up a different phase during transmission through the QD-cavity system. In the weak coupling regime, but often also in the strong coupling regime, the individual Jaynes Cummings dressed states cannot be resolved spectrally because $g \lesssim \kappa$. However, the CQED system is still photon-number sensitive, which implies lifetime-dependent Jaynes Cummings effects in the weak coupling regime: the decay rate of the CQED system increases with the number of photons in the cavity [34, 35]. As consequence, higher photon-number states have a modified interaction cross section and experience a reduced phase shift. The dip in P_2 in Fig. 4 is already very close to the cross-polarization angle $\theta_{out} = -45°$, while the dips for higher photon number states $P_{n>2}$ is

indistinguishable from $\theta_{out} = -45°$.

We add that, while single Fock states have an undefined phase, superpositions of different Fock states, such as in different polarization modes have a well defined relative phase. This is also the basis of a recent observation of quadrature squeezing in the resonance fluorescence of a single quantum dot [36], where orthogonal polarizations have been used to obtain a phase-stable local oscillator. We have calculated the amount of quadrature squeezing of the transmitted light in our system and predict slightly larger squeezing amplitudes than those observed in [36], which is expected due to the cavity enhancement in our system. However, photon correlations as strong as we report here can only be achieved by coupling a QD to a high-quality optical cavity, which has to be sufficiently polarization degenerate to enable our purification technique: the quantum dot transition has to couple simultaneously to both orthogonal polarizations, for details see the supplemental information [24].

In conclusion, we found that the nonlinear response of a lossy cavity-quantum dot system can be strongly enhanced by postselection of a particular polarization state. This leads to interference between Fock states that experienced different modifications by the QD nonlinearity, and results in strong photon correlations of the transmitted light. As the underlying effect, interference of the two polarizations modes leads to high-fidelity cancellation of the single-photon transmission for the special polarization pre- and postselection. By correlating the results with a theoretical model, we found indications of photon-number sensitive Jaynes-Cummings physics in the weak coupling regime of CQED.

[1] Imamoglu, A., Schmidt, H., Woods, G. & Deutsch, M. Strongly Interacting Photons in a Nonlinear Cavity. *Phys. Rev. Lett.* **79**, 1467 (1997).

[2] Bonato, C. *et al.* CNOT and Bell-state analysis in the weak-coupling cavity QED regime. *Phys. Rev. Lett.* **104**, 160503 (2010).

[3] Kimble, H. J. The quantum internet. *Nature* **453**, 1023 (2008).

[4] Imamoglu, A. *et al.* Quantum Information Processing Using Quantum Dot Spins and Cavity QED. *Phys. Rev. Lett.* **83**, 4204 (1999).

[5] Jaynes, E. & Cummings, F. Comparison of quantum and semiclassical radiation theories with application to the

beam maser. *Proc. IEEE* **51**, 89 (1963).

[6] Kubanek, A. *et al.* Two-Photon Gateway in One-Atom Cavity Quantum Electrodynamics. *Phys. Rev. Lett.* **101**, 203602 (2008).

[7] Birnbaum, K. M. *et al.* Photon blockade in an optical cavity with one trapped atom. *Nature* **436**, 87 (2005).

[8] Dayan, B. *et al.* A Photon Turnstile Dynamically Regulated by One Atom. *Science* **319**, 1062 (2008).

[9] Schuster, I. *et al.* Nonlinear spectroscopy of photons bound to one atom. *Nat. Phys.* **4**, 382 (2008).

[10] Kasprzak, J. *et al.* Up on the Jaynes–Cummings ladder of a quantum-dot/microcavity system. *Nat. Mater.* **9**, 304 (2010).

[11] Faraon, A., Majumdar, A. & Vučković, J. Generation of nonclassical states of light via photon blockade in optical nanocavities. *Phys. Rev. A* **81**, 033838 (2010).

[12] Faraon, A. *et al.* Coherent generation of non-classical light on a chip via photon-induced tunnelling and blockade. *Nat. Phys.* **4**, 859 (2008).

[13] del Valle, E., Gonzalez-Tudela, A., Laussy, F. P., Tejedor, C. & Hartmann, M. J. Theory of Frequency-Filtered and Time-Resolved N -Photon Correlations. *Phys. Rev. Lett.* **109**, 183601 (2012).

[14] Muñoz, C. S. *et al.* Emitters of N-photon bundles. *Nat. Photonics* **8**, 550 (2014).

[15] Reinhard, A. *et al.* Strongly correlated photons on a chip. *Nat. Photonics* **6**, 93 (2012).

[16] Majumdar, A., Bajcsy, M. & Vučković, J. Probing the ladder of dressed states and nonclassical light generation in quantum-dot–cavity QED. *Phys. Rev. A* **85**, 041801 (2012).

[17] Rundquist, A. *et al.* Nonclassical higher-order photon correlations with a quantum dot strongly coupled to a photonic-crystal nanocavity. *Phys. Rev. A* **90**, 023846 (2014).

[18] Müller, K. *et al.* Coherent Generation of Nonclassical Light on Chip via Detuned Photon Blockade. *Phys. Rev. Lett.* **114**, 233601 (2015).

[19] McNeil, K. & Walls, D. Possibility of observing enhanced photon bunching from two photon emission. *Phys. Lett. A* **51**, 233 (1975).

[20] Yoshie, T. *et al.* Vacuum Rabi splitting with a single quantum dot in a photonic crystal nanocavity. *Nature* **432**, 200 (2004).

[21] Reithmaier, J. P. *et al.* Strong coupling in a single quantum dot-semiconductor microcavity system. *Nature* **432**, 197 (2004).

[22] Hu, C. Y., Munro, W. J., O'Brien, J. L. & Rarity, J. G. Proposed entanglement beam splitter using a quantum-dot spin in a double-sided optical microcavity. *Phys. Rev. B* **80**, 205326 (2009).

[23] Arnold, C. *et al.* Macroscopic rotation of photon polarization induced by a single spin. *Nat. Commun.* **6**, 6236 (2015).

[24] See Supplemental Material.

[25] Strauf, S. *et al.* High-frequency single-photon source with polarization control. *Nat. Photonics* **1**, 704 (2007).

[26] Bakker, M. P. *et al.* Polarization degenerate micropillars fabricated by designing elliptical oxide apertures. *Appl. Phys. Lett.* **104**, 151109 (2014).

[27] Coldren, L. A., Thibeault, B. J., Hegblom, E. R., Thompson, G. B. & Scott, J. W. Dielectric apertures as intracavity lenses in vertical-cavity lasers. *Appl. Phys. Lett.* **68**, 313 (1996).

[28] Bonato, C. *et al.* Tuning micropillar cavity birefringence by laser induced surface defects. *Appl. Phys. Lett.* **95**, 251104 (2009).

[29] Bakker, M. P. *et al.* Polarization degenerate solid-state cavity quantum electrodynamics. *Phys. Rev. B* **91**, 115319 (2015).

[30] Armen, M. A. & Mabuchi, H. Low-lying bifurcations in cavity quantum electrodynamics. *Phys. Rev. A* **73**, 063801 (2006).

[31] Johansson, J., Nation, P. & Nori, F. QuTiP 2: A Python framework for the dynamics of open quantum systems. *Comput. Phys. Commun.* **184**, 1234 (2013).

[32] Giesz, V. *et al.* Coherent control of a solid-state quantum bit with few-photon pulses. *pre-print arXiv:1512.04725* (2015).

[33] We calculate this inside of the cavity to clearly demonstrate the effect; in reality, the output coupler mirror would reshape the photon number distribution before the polarizer acts.

[34] Illes, E., Roy, C. & Hughes, S. Spectral multiphoton effects and quantum anharmonicities in dissipative cavity-QED systems via off-resonant coherent excitation. *Optica* **2**, 689 (2015).

[35] Laussy, F. P., del Valle, E., Schrapp, M., Laucht, A. & Finley, J. J. Climbing the Jaynes–Cummings ladder by photon counting. *J. Nanophoton.* **6**, 061803 (2012).

[36] Schulte, C. H. H. *et al.* Quadrature squeezed photons from a two-level system. *Nature* **525**, 222 (2015).

Purification of a single photon nonlinearity
Supplemental Material

I. SAMPLE STRUCTURE

The samples under study are grown by molecular beam epitaxy on a GaAs [100] substrate. Two distributed Bragg reflectors (DBR) surround a $\sim 5\lambda$ thick cavity [1] containing in the center InGaAs self-assembled quantum dots (QDs) and an oxide aperture for transverse confinement. The top DBR mirror consists of 26 pairs of $\lambda/4$ thick GaAs / $Al_{0.90}Ga_{0.10}As$ layers, while the bottom mirror has 13 pairs of GaAs / AlAs layers and 16 pairs of GaAs / $Al_{0.90}Ga_{0.10}As$ layers. The aperture is made of a 10 nm thick AlAs layer which is embedded between 95 nm $Al_{0.83}Ga_{0.17}As$ and 66 nm thick $Al_{0.75}Ga_{0.25}As$. After wet chemical oxidation this enables an intra-cavity lens for transverse mode confinement. In the paper, we discuss two quantum dots, QD A and QD B, in two different samples. QD A is separated by a 20 nm thick GaAs tunnel barrier from the n-doped GaAs:Si (2.0×10^{18} cm^{-3}), while QD B is separated by a 35 nm tunnel barrier to reduce co-tunneling induced decoherence.

II. THEORETICAL MODELLING

A. Jaynes-cumming quantum master equation

We describe the QD-cavity system via an extended version of a two level system in an optical cavity, which is driven by a classical coherent laser field. The quantum description, based on the application of a unitary transformation to transform the Hamiltonian from a time dependent to a time independent form and the rotating wave approximation, results in the following Hamiltonian ($\hbar = 1$)[2, 3]:

$$
\begin{aligned}
H = {}& \left(\omega_L - \omega_c\right) \hat{a}_X^\dagger \hat{a}_X + \left(\omega_L - \omega_c\right) \hat{a}_Y^\dagger \hat{a}_Y + \left(\omega_L - \omega_{QD}^X\right) \hat{\sigma}_X^\dagger \hat{\sigma}_X + \left(\omega_L - \omega_{QD}^Y\right) \hat{\sigma}_Y^\dagger \hat{\sigma}_Y \\
& + g_Y \left(\hat{\sigma}_Y \hat{a}_Y^\dagger + \hat{\sigma}_Y^\dagger \hat{a}_Y\right) + g_X \left(\hat{\sigma}_X \hat{a}_X^\dagger + \hat{\sigma}_X^\dagger \hat{a}_X\right) + \frac{\eta}{2} \left[e_x' \left(\hat{a}_X^\dagger + \hat{a}_X\right) + e_y' \left(\hat{a}_Y^\dagger + \hat{a}_Y\right)\right]
\end{aligned}
$$

Here ω_c is the cavity resonance frequency and $\omega_{QD}^{X/Y}$ are the fine-structure-split QD transition frequencies. $\hat{a}_{X/Y}^\dagger$ is the photon creation operator for a photon in X/Y polarization, and $\hat{\sigma}_{X/Y}^\dagger$ creates an X/Y polarized neutral exciton. The terms with coupling constants $g_{X/Y}$ describe the interaction between a QD transition and the cavity field. This Hamiltonian is designed for a polarization degenerate cavity. The last term describes the driving of the cavity by an external linearly polarized coherent laser field, where η^2 is proportional to the incident intensity [4], and the Jones vector $\left(e_x', e_y'\right)$ describes the incident light polarization.

Next we write down a quantum master equation for our Hamiltonian and include Lindblad-type dissipation for the cavity decay rate κ, the population relaxation rate $\gamma_{||}$ and the total pure dephasing rate γ^*.

$$
\frac{d\rho}{dt} = \mathfrak{L}\rho = -i\left[\hat{H}, \rho\right] + \sum_{j=X,Y} \frac{\kappa}{2}\mathfrak{D}[\hat{a}_j]\rho + \frac{\gamma_{||}}{2}\mathfrak{D}[\hat{\sigma}_j]\rho + \frac{\gamma^*}{4}\mathfrak{D}[\hat{\sigma}_{zj}]\rho, \tag{1}
$$

Where ρ is the density matrix of the QD-cavity system, $\mathfrak{L}$ is the Liouvillian superopererator for QD-cavity density matrix and $\mathfrak{D}[\hat{o}]\rho \equiv 2\hat{o}\rho\hat{o}^\dagger - \hat{o}^\dagger\hat{o}\rho - \rho\hat{o}^\dagger\hat{o}$ results in Lindblad type dissipation. Here $\hat{\sigma}_{zj}$ is defined as $\frac{1}{2}\left(\hat{\sigma}_j^\dagger\hat{\sigma}_j - \hat{\sigma}_j\hat{\sigma}_j^\dagger\right)$. This Lindblad-type master equatition in Eq. 1 is based on the validity of several additional approximations (see for instance [5]), where we point out a few: (1) full separability of the system and the environment at $t = 0$, and (2) the state of the environment does not change significantly under interaction with the system, i.e., the interaction is weak, and the system and environment remain separable throughout the evolution. Last, we assume (3) that the environment has no memory on the time scale of the system (Markov approximation). Those approximations are justified as we only discuss photonic interaction with the environment here, which is very weak. We are interested in the steady state solution for ρ, and solve $\mathfrak{L}\rho = 0$, using the numerical methods provided by the software package QUTIP [6].

B. Transmission and photon correlations

The cavity transmittivity is calculated by $T = \text{Tr}\left[\rho_0 \left(e_1 \hat{a}_X^\dagger + e_2 \hat{a}_Y^\dagger\right)\left(e_1 \hat{a}_X + e_2 \hat{a}_Y\right)\right] = \text{Tr}\left(\rho_0 \hat{a}^\dagger \hat{a}\right)$, where (e_1, e_2) describes the output polarizer Jones vector, and ρ_0 is the steady-state density matrix of the system. We investigate the photon correlations by calculating the second-order correlation function, which is independent of mirror loss and can therefore be calculated directly from the intracavity photon operators $\langle \hat{a}^\dagger \hat{a}\rangle$. The second-order correlation function is given by $g^2(\tau) = \frac{\langle \hat{a}^\dagger(0)\hat{a}^\dagger(\tau)\hat{a}(\tau)\hat{a}(0)\rangle}{\langle \hat{a}^\dagger(0)\hat{a}(0)\rangle^2}$ with the time dependent photon creation operator $\hat{a}^\dagger(\tau)$. In order to solve the time dependence of the operator $\hat{a}^\dagger(\tau)$, we assume that the effect of the operator $\mathfrak{L}$ is small and the eigenvalues are nondegenerate, which allows us to write $\hat{a}^\dagger(\tau)$ as $\hat{a}^\dagger e^{\mathfrak{L}\tau}$. The effect of the operator $\mathfrak{L}$ is small if it acts on a steady-state density matrix [7].

III. ESTIMATION OF MODEL PARAMETERS

For estimation of the parameters, we fit the theory above discussed to the experimental transmission data for 6 different output polarizations for $\theta_{in} = 45°$ (excitation of both QD transitions). The result in Fig. S1 shows excellent agreement between experiment (blue curve) and theory (red curve). We obtain for QD A the best-fit parameters $\kappa = 69$ ns^{-1}, $g = 15$ ns^{-1}, $\gamma^{||} = 3.5$ ns^{-1}, $\gamma^* = 6$ ns^{-1}, $f_{QD}^{X/Y} = -1.5/1.3$ GHz.
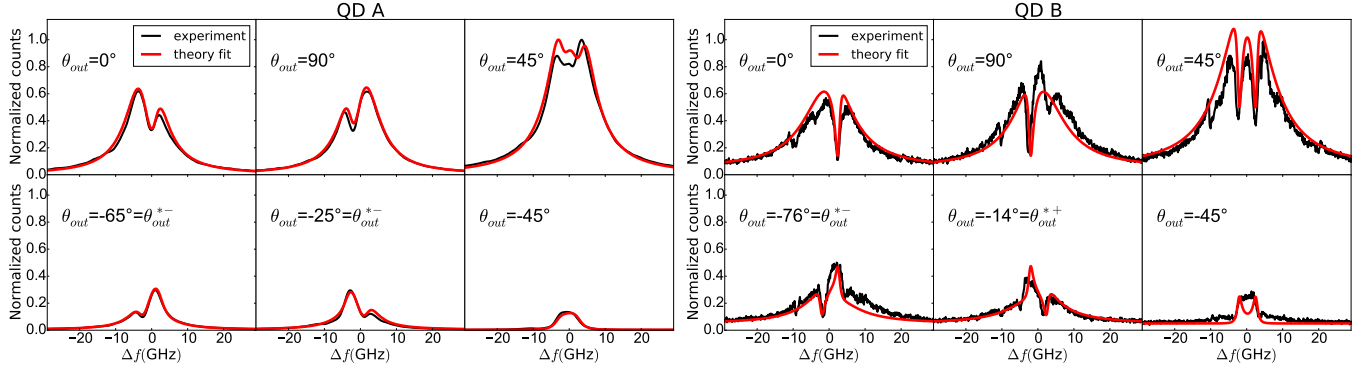

Figure S1. Experimental data (black) and the theoretical fit (red) for QD A (left panel) and QD B (right panel). The input polarization was set to $\theta_{in} = 45°$ for both cases and θ_{out}^{*+} and θ_{out}^{*-} indicate the special polarization angles.

For QD B, we obtained the fitting parameters $\kappa = 105$ ns^{-1}, $g = 14$ ns^{-1}, $\gamma^{||} \approx 1.0$ ns^{-1}, $\gamma^* \approx 0.7$ ns^{-1}, $f_{QD}^{X/Y} = -2.0/2.4$ GHz. As we discuss below, the strongly reduced pure dephasing rates leads to much higher photon correlations for QD B. The experimental results for QD B do not corresponds as nice to the theory as those of QD A; the reason for this is that the cavity of QD B is not fully polarization degenerate. This is most clear under the cross polarization configuration ($\theta_{out} = -45°$) at around $\Delta f = 0$. Furthermore, the fits for QD B are complicated by the presence of another QD in the same cavity ($\theta_{out} = 90°$, at around -10 GHz). Notice that due to different system parameters the special polarization angles for QD A and QD B differ by $11°$.

IV. ADDITIONAL PHOTON CORRELATION DATA

Here we show additional comparison of measured and calculated photon correlation data for QD B. This data supports Fig. 1c in the main text, and is obtained analogous to the data presented in Fig. 3. Fig. S2 shows the false-color map of $g^2(0)$ as function of the output polarization θ_{out} and QD detuning. Similar to QD A (Fig. 3) we again obtain good agreement between experiment and theory and observe strong photon bunching for the special polarization case. The main difference between QD A (Fig. 3) and QD B (Fig. S2) is that, here for QD B, the obtained bunching is much larger. Again, the difference between theory and experiment in absolute numbers in Fig. S2 is due to the detector jitter (see below Fig. S5).
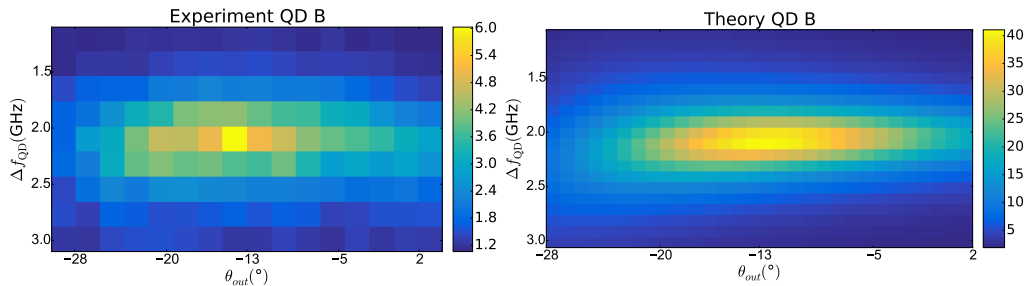

Figure S2. Experimental (left) and theoretical (right) two-photon correlation $g^2(0)$ as a function of QD frequency Δf_{QD} and output polarization θ_{out}. The experimental values of $g^2(0)$ are reduced by the detector jitter of 500 ps.

Next, we address the question, which parameters are responsible for the much stronger photon bunching obtained for QD B compared to QD A? To investigate this, we have performed numerical experiments tuning the system parameters, shown in Fig. S3.
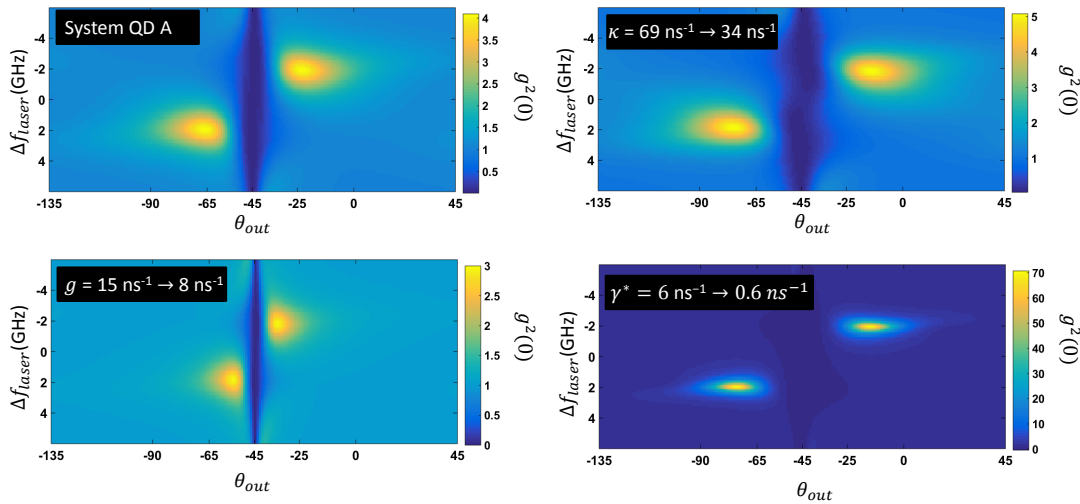

Figure S3. Predicted false-color plots of $g^2(0)$ for different system parameters. In each plot one parameter is changed to a different value compared to the best fitting parameters for QD A. The changed parameters are indicated in the plots. Note the changes in the color scales.

In the false color plots of Fig. S3 we show the theoretical prediction of $g^2(0)$ of QD A while scanning the laser over the cavity resonance and changing the output polarization θ_{out}. We show that by decreasing κ and g to half of their original value, the effect on $g^2(0)$ is marginal as compared to when we change the pure dephasing γ^*. A smaller g gives a slightly smaller photon bunching and a lower κ gives a slightly larger bunching simply because the cooperativity increases or decreases. However, once the pure dephasing γ^* is reduced from 6 to 0.5, $g^2(0)$ increases to a value of ≈ 70. This corresponds well to the measurement of QD B in Fig. 1c where we have a pure dephasing of $\gamma^* \approx 0.7$ and measure a $g^2(0) \approx 25$, which correponds to $g^2(0) \gtrsim 40$ after deconvolution. We note that for these extreme cases of photon bunching, the exact $g^2(0)$ value is very sensitive to the exact model parameters in the numeric calculations.

We conclude that small pure dephasing is key to obtain strong photon bunching in CQED systems.

V. QD LEVELS

In our neutral quantum dots, the electron-hole exchange interaction leads to two fine-structure-split optical transitions. Fig S4 shows the prediction for $g^2(0)$ when one QD transitions is removed. We see, as expected, that the strong photon bunching now appears only around the remaining QD transition, where the purification mechanism operates. However, with a hypothetical QD without fine structure splitting, the two QD transitions would have exactly the same energy and the purification mechanism does not work, precluding the observation of strong photon bunching.
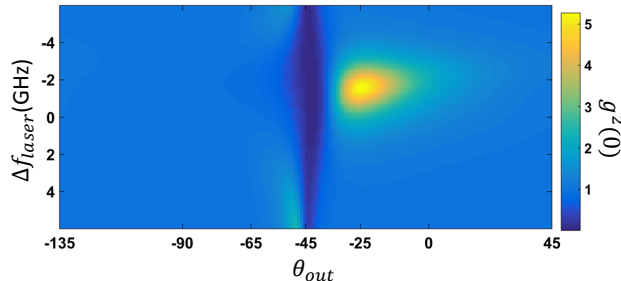

Figure S4. Theoretical data of the second-order correlation function as a function of the QD frequency and output polarization if one of the QD transition is removed from the simulations.

VI. DETECTOR RESPONSE

In order to show that the true two-photon correlations are much stronger than the raw experimental data suggests, we now present details on the convolution of the theoretical $g^2(\tau)$ data with the single photon counter (SPC) detector response. We use two detectors with 50 ps and 500 ps detector jitter, which was determined by measuring photon correlations of a picosecond Ti:Sapphire laser oscillator. As shown in Fig S5 we observe very good agreement between the convoluted theoretical prediction and the experimental data for both QD A en QD B. Since count rates were higher for QD B, we could also perform the experiment with a less sensitive 50 ps jitter detector, which again agrees very well to theory. This clearly shows that our $g^2(\tau)$ measurements are severly reduced by the detector jitter of the single photon counters, but that we can fully deconvolute this effect.
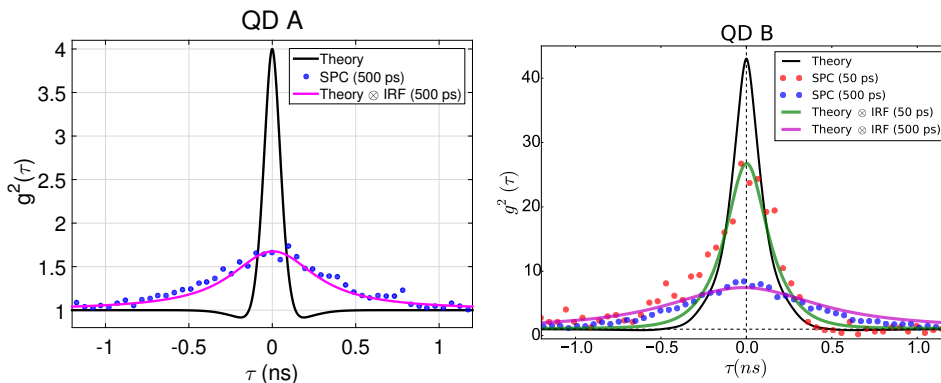

Figure S5. Comparison of the theoretical data with and without taking care of detector jitter, and the experimental $g^2(\tau)$ data for QD A (left) and QD B (right). The agreement between theory and experiment is excellent.

VII. PHOTON CORRELATIONS AND CAVITY QUALITY

Here we show that the cavity is essential to obtain such strong photon correlations as we have observed experimentally. For this we conduct numerical simulations for various cavity decay rates κ. In order to isolate the effect of κ, we have to optimize for each value of κ the laser frequency and the output polarization to find the special polarization angle and thereby the maximum in the $g^2(0)$ landscape. Next to this we also need to keep the internal mean photon number constant by increasing the incident laser power for a higher value of κ. In order to do this we optimized the power coupling parameter η for each value of κ, so that the mean photon number of the outgoing light (for parallel polarization $\theta_{in} = \theta_{out} = 45°$) on the cavity resonance for an empty cavity remains constant. The result is shown in Fig. S6: In the case of almost no cavity (large κ), only very small $g^2(0)$ values are obtainable, while in good cavities (small κ), extreme values of $g^2(0)$ are possible. The other parameters for simulation of Fig. S6 are similar to those of QD B.
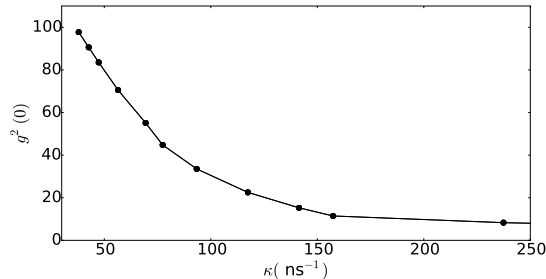

Figure S6.   Calculated maximal (i.e., for special polarizer angles) $g^2(0)$ for different cavity decay rates. A good cavity with low κ is needed in order to reach the extreme bunching values $g^2(0)$.

[1] Bakker, M. P. *Cavity quantum electrodynamics with quantum dots in microcavities.* Ph.D. thesis, University of Leiden (2015).
[2] Jaynes, E. & Cummings, F. Comparison of quantum and semiclassical radiation theories with application to the beam maser. *Proc. IEEE* **51**, 89 (1963).
[3] Arnold, C. *et al.* Macroscopic rotation of photon polarization induced by a single spin. *Nat. Commun.* **6**, 6236 (2015).
[4] Tang, J., Geng, W. & Xu, X. Quantum Interference Induced Photon Blockade in a Coupled Single Quantum Dot-Cavity System. *Sci. Rep.* **5**, 9252 (2015).
[5] Johansson, J., Nation, P. & Nori, F. QuTiP: An open-source Python framework for the dynamics of open quantum systems. *Comput. Phys. Commun.* **183**, 1760 (2012).
[6] Johansson, J. R., Nation, P. D. & Nori, F. QuTiP 2: A Python framework for the dynamics of open quantum systems. *Comput. Phys. Commun.* **184**, 1234 (2013).
[7] Gardiner, C. & Zoller, P. *Quantum Noise* (Springer, 2004).